Available online at www.sciencedirect.com
SCIENCE DIRECT®
Journal of Catalysis 231 (2005) 314–330
JOURNAL OF CATALYSIS
www.elsevier.com/locate/jcat

Selective reduction of NO with Fe-ZSM-5 catalysts of low Fe content I. Relations between active site structure and catalytic performance

Michael Schwidder [a], M. Santhosh Kumar [b], Konstantin Klementiev [a], Marga Martina Pohl [b], Angelika Brückner [b], Wolfgang Grünert [a,*]

[a] *Lehrstuhl für Technische Chemie, Ruhr-Universität Bochum, D-44780 Bochum, Germany*
[b] *Institut für Angewandte Chemie Berlin-Adlershof e.V., Richard-Willstätter-Str. 12, D-12489 Berlin, Germany*

Received 27 October 2004; revised 24 January 2005; accepted 26 January 2005

Available online 17 March 2005

Abstract

Fe-ZSM-5 catalysts (0.2–1.2 wt% Fe) were prepared by an exchanging of Na-ZSM-5 with Fe^{2+} ions formed by the dissolution of iron in acidic medium, and characterized by UV–vis, EPR, and X-ray absorption spectroscopy and by TPR and TEM. Their catalytic properties were investigated for the selective catalytic reduction (SCR) of NO by isobutane (2000 ppm NO, 2000 ppm isobutane, 3% O_2, 42,000 h^{-1}) or by NH_3 (1000 ppm NO, 1000 ppm NH_3, 1% O_2, 750,000 h^{-1}). The catalysts were highly active in both reactions, competing favorably with catalysts prepared by chemical vapor deposition of $FeCl_3$ into H-ZSM-5. The spectroscopic studies showed that at Fe contents less than or equal to 0.3 wt%, ca. 95% of the iron was present in mononuclear sites of different coordination. At higher Fe contents, small oligomeric clusters coexisted with mononuclear sites, and at 1.2% Fe, large, poorly ordered Fe oxide aggregates were also detected. By correlation of the activities with the concentration of Fe sites as determined from UV–vis spectra, it was established that mononuclear Fe ions are active sites for both SCR reactions, but oligomers contribute as well. At the same time, oligomers (and aggregate surfaces) are more active in unselective oxidation of the reductant, which limits the temperature window of selective NO reduction. This unselective attack by clustered species occurs at low temperatures with isobutane; hence the best performance was found for a catalyst of low Fe content (0.3 wt%), which is at variance with previous optimization strategies. With NH_3, the unselective attack occurs at a much higher temperature; hence the best catalysts for NH_3-SCR are those with the highest exposure of Fe sites.

Keywords: $DeNO_x$; Fe-ZSM-5; Isobutane; Ammonia; EXAFS; UV–vis spectroscopy; EPR spectroscopy; Active sites

1. Introduction

Iron-modified ZSM-5 has recently received much attention in catalysis research because of its promising activity in numerous reactions of industrial and environmental relevance, such as selective oxidations with N_2O [1,2], the decomposition or selective reduction of nitrous oxide [3–5], the selective catalytic reduction (SCR) of NO_x by ammonia [6–8] or hydrocarbons [9–14], and the selective oxidation of NH_3 to N_2 [15]. For the selective NO reduction, catalysts prepared by chemical vapor deposition (CVD) of anhydrous iron(III) chloride onto the H-form of the zeolite [10] have been shown to yield high activities most reproducibly. In the other reactions, a lower Fe content is more favorable, and the active species are sometimes developed only during a high-temperature treatment of the as-prepared catalysts.

Although much effort has been invested in the characterization of the iron sites in these catalysts, with a multitude of physicochemical techniques having been applied by now, the nature of the active sites for most of the reactions mentioned above is still under debate. Thus, intra-zeolite binuclear oxygen-bridged Fe sites, for which models were derived from EXAFS studies [16,17], have been claimed to be active sites for hydrocarbon-SCR [10,11], and binu-

* Corresponding author. Fax: +49 234 321 4115.
E-mail address: w.gruenert@techem.ruhr-uni-bochum.de (W. Grünert).

0021-9517/$ – see front matter
doi:10.1016/j.jcat.2005.01.031

clear sites are also proposed to activate the oxygen deposited from N_2O (α-oxygen) [2,18]. On the other hand, mononuclear sites (not necessarily of the same structure) have been suggested to catalyze benzene oxidation by N_2O [19–21], N_2O decomposition [22], and hydrocarbon-SCR [23]. A major problem with Fe-ZSM-5 catalysts, particularly at high Fe content, is a tendency of the Fe species to cluster into aggregates, which leads to a very heterogeneous distribution of iron species in these materials [13,24,25]. In previous studies, our groups proposed that in Fe-ZSM-5 prepared by CVD of $FeCl_3$, the active sites for isobutane-SCR are minority sites [13], probably oligomers of low nuclearity *including* mononuclear sites [13,24,26]. Cooperative studies of N_2O decomposition over Fe-ZSM-5 with iron sites prepared by steam extraction of framework Fe led to the conclusion that N_2O decomposition proceeds on oligonuclear aggregates, whereas the reduction of N_2O by CO or propane can proceed on both isolated and oligomeric sites [27,28].

The lower Fe contents used in catalysts for phenol oxidation and several studies of N_2O decomposition and reduction bear the promise of a more homogeneous structure of the Fe sites present, although recent characterization studies have shown that it is impossible even then to completely escape aggregation [27,28]. It has been demonstrated in [24, 26,29] that a high Fe content is not a prerequisite for high activities in isobutane-SCR. However, the mechanochemical preparation route described in [26] did not turn out to be flexible enough to make available a series of Fe-ZSM-5 catalysts with varying distribution of the sites observed in catalysts with high Fe content [24]: isolated sites of different coordination sphere, oligomeric Fe oxo species of different nuclearity, and large Fe oxide aggregates.

In a study of various preparation procedures, the "Improved Liquid Ion Exchange" (ILIE) originally proposed by Long and Yang [30] was found to do the best at living up to these expectations [31]. This preparation method, which involves treatment of NH_4-ZSM-5 with Fe^{2+} ions generated in situ by the dissolution of iron powder in diluted hydrochloric acid under anaerobic conditions, was modified with regard to the quantity of iron powder used to obtain a series of Fe-ZSM-5-catalysts with iron contents down to 0.2 wt%. In the present paper, an extended study of the structural and catalytic properties of these catalysts is presented. In the first section, catalytic and (ex situ) characterization results are reported. The characterization has been performed with several techniques, including X-ray absorption spectroscopy (XAFS), electron paramagnetic resonance (EPR), UV–vis spectroscopy, temperature-programmed reduction by hydrogen (H_2-TPR), transmission electron microscopy (TEM), and pore volume determination by N_2 physisorption. The information about the nature of the Fe species in the catalysts has been correlated with activities in the selective reduction of nitric oxide with isobutane and ammonia, which makes it possible to draw conclusions about the nature of the active sites in these reactions. In the second section [32], in situ UV–vis and EPR studies are described, which give deeper insight into the behavior of the iron sites during catalysis. The present paper is a full account of data that have been preliminarily communicated in [33].

2. Experimental

2.1. Materials

The parent Na-ZSM-5 (Si/Al = 14) sample was kindly supplied by Chemiewerk Bad Köstritz (Germany). Iron was introduced with an Improved Liquid Ion Exchange technique slightly different from that of Long and Yang [30]. For this purpose 6 g of Na-ZSM-5, a varying amount (Table 1) of Fe powder (Merck, Goodfellow), and 600 ml of deionized water were charged into a double-necked flask equipped with a gas-inlet tube and a magnetic stirrer. After the flask was flushed with argon, 6 ml of concentrated hydrochloric acid was slowly added to the mixture, resulting in a HCl concentration of 0.1 mol l^{-1}. After the liquid was stirred for 5 days it was removed, and the prepared Fe-ZSM-5-samples were washed with deionized water. Finally the catalysts were dried at room temperature and subsequently calcined in flowing air according to the following temperature protocol: first the temperature was raised from room temperature to 423 K at 2 K min^{-1} and, after a 15-min isothermal period, the temperature ramp was continued at 5 K min^{-1} to 873 K, where the samples were left for 2 h.

In several places reference will be made to a Fe-ZSM-5 material prepared by CVD of $FeCl_3$ into H-ZSM-5, which was studied earlier in our group [13,24] and was labeled A(CVD, W1, C5) in the earlier papers. It contains ∼ 5 wt% Fe and is referred to here as Fe-Z(CVD). Another reference catalyst prepared by the mechanochemical preparation route described in [26] and containing 0.5 wt% Fe is referred to here as Fe-Z(MR).

2.2. Determination of iron contents

The iron contents of the Fe-ZSM-5-samples were determined by the ICP-OES method. For this purpose we digested 50 mg of each sample by melting a mixture with 250 mg of $LiBO_2$ at 1273 K and subsequently dissolving the melt in

Table 1
Prepared Fe-ZSM-5-samples, their chemical composition, and micropore volume obtained from N_2-physisorption

Sample	Amount of iron used in preparation (g/g zeolite)	Iron content (wt%)	n_{Fe}/n_{Al}	Micropore volume ($cm^3\,g^{-1}$)
Na-ZSM-5	–	0.05	0.008	0.15
Fe-Z(1.2)	0.5	1.2	0.195	0.12
Fe-Z(0.7)	0.333	0.7	0.114	0.13
Fe-Z(0.6)	0.2	0.6	0.097	0.14
Fe-Z(0.3)	0.1	0.3	0.048	0.13
Fe-Z(0.2)	0.05	0.2	0.033	0.15

diluted nitric acid. ICP-OES measurements were carried out with a UNICAM PU-7000-spectrometer. We confirmed the results by comparison with results deduced from the XAFS spectra of these samples by comparing the edge heights obtained with the specific absorption coefficient of iron on the basis of Lambert–Beer's law.

2.3. Catalysis

The SCR of NO with isobutane was carried out in a catalytic micro-flow quartz reactor at temperatures between 823 and 523 K, with reaction temperatures decreasing during the measurement sequence. Before each catalytic run, 150 mg of catalyst was heated in flowing He to 823 K at 5 K min^{-1} and left at this temperature for 30 min. After that, a feed mixture of 2000 ppm NO, 2000 ppm isobutene, and 3% O_2 in He was directed through the catalyst bed at a flow rate of 154 ml min^{-1}, which resulted in a GHSV of 42,000 h^{-1}. To relate the present study to our earlier work [13,24,26,29], additional experiments were carried out with a mixture of 1000 ppm NO, 1000 ppm isobutane, and 2% O_2 in He, where the GHSV was adjusted to 30,000 h^{-1}. These sets of conditions are referred to here as set A- and set B-isobutane, respectively.

The SCR of NO with ammonia was performed under similar conditions; however, the temperatures were varied between 873 and 423 K. The feed gas composition was 1000 ppm NO, 1000 ppm NH_3, and 2% O_2 in He at a GHSV of 750,000 h^{-1} (10 mg catalyst, 183.3 ml min^{-1} gas feed; set A-NH_3). In addition, results obtained with a GHSV of 30,000 h^{-1} (set B-NH_3) are reported as well. The composition of the effluent gas was analyzed by calibrated mass spectrometry in the case of isobutane-SCR and a combination of photometric devices for the detection of NO, NO_2, and NH_3 in the case of NH_3-SCR (for part of the work supported by the mass-spectrometric detection of N_2O). In both cases, we also used gas chromatography to analyze the quantity of nitrogen released to trace the possible formation of NO_2 or N_2O in significant amounts by setting up a nitrogen balance. This balance typically rendered values between 95 and 105%.

2.4. Determination of pore volumes

Pore volumes were determined from N_2 physisorption data with the BJH method [34]. Nitrogen physisorption was carried out with an Autosorb-1-MP device (Quantachrome). Before each experiment the samples were dehydrated at 573 K for 2 h.

2.5. Temperature-programmed reduction

Temperature-programmed reduction was performed with a gas mixture containing 4.2 vol% H_2 in He. Before each experiment, the samples were heated at 823 K for 2 h in flowing synthetic air. The reduction was carried out with a 10 K min^{-1} temperature ramp between room temperature and 1073 K. The hydrogen content of the effluent gas was measured with a Hydros instrument (Fisher–Rosemount).

2.6. X-ray absorption spectroscopy

X-ray absorption measurements (Fe K-edge at 7112 keV) were carried out at Hasylab beamline E4 (Hamburg/Germany), with a Si(111) double crystal monochromator for energy tuning. Absorption spectra were measured in transmission mode and in fluorescence mode in the case of samples with low iron loading. In both cases samples were diluted with polyethylene and pressed into wafers of suitable thickness. When measurements were made in transmission mode, the intensity decrease in the beam was detected by ion chambers that were installed before and after the sample. An iron metal foil was measured at the same time (between the second and an additional third ion chamber) for energy calibration. For measurements in fluorescence mode, a 7-pixel Si(Li) detector was used. In all cases measurements were carried out at LN_2 temperature. Data treatment of the EXAFS part of the spectra was accomplished with the software VIPER for Windows [35]. The pre-edge background of the spectra was subtracted according to Victoreen's law, and the EXAFS function $\chi = (\mu - \mu_0)/\mu_0$ was evaluated relative to an atomic background μ_0 estimated with the smoothing-spline technique. For preliminary determination of the edge position, the inflection point of the pre-edge peak was used to avoid fluctuations imposed by slight changes in the shape of the edge itself. In the model fits, this led to numerical values of the E_0 correction that were higher than usual (see Tables 2–4). Radial distribution functions were obtained by Fourier transformation of the k^2-weighted EXAFS functions. Fitting of the Fourier-filtered EXAFS functions was carried out on the basis of scattering amplitudes and phases obtained from the code FEFF8.1 [36]. To minimise the number of free parameters, equal backscatterers were fitted with the same E_0 shift wherever possible (variations of ±0.5 eV admitted). A less stringent constraint was imposed on the Debye–Waller factor ($0.001\ \text{Å}^{-2} < \sigma < 0.015\ \text{Å}^{-2}$).

2.7. UV–vis–DRS-spectroscopy

UV–vis-measurements were performed with a Cary 400 spectrometer (Varian) equipped with a diffuse reflectance accessory (Harrick). For light absorption reduction, samples were diluted by α-Al_2O_3 (calcined for 4 h at 1473 K) in a ratio of 1:10. Deconvolution of the UV–vis spectra into subbands was performed by the computer program GRAMS/32 (Galactic).

2.8. Electron paramagnetic resonance

EPR spectra in the X-band ($\nu \approx 9.5$ GHz) were recorded with a CW spectrometer (ELEXSYS 500-10/12; Bruker) at a microwave power of 6.3 mW, a modulation frequency

of 100 kHz, and a modulation amplitude of 0.5 mT. The magnetic field was measured in reference to the standard 2,2-diphenyl-1-picrylhydrazyl-hydrate (DPPH). For temperature-dependent measurements in the range from 80 to 293 K, a commercial variable-temperature control unit (Bruker) and a conventional EPR sample tube were used, while in situ-EPR measurements during calcination at higher temperatures were performed in a home-made EPR flow reactor as indicated in [24].

2.9. Transmission electron microscopy

TEM/EDX measurements were performed at 200 keV with a CM 20 microscope (Philips) equipped with an EDX accessory (EDAX PV 9900). Samples were dispersed on a lacey carbon film.

3. Results

3.1. Iron contents and pore volumes

The iron contents of the Fe-ZSM-5-catalysts and the calculated Fe/Al ratios are listed in Table 1. As shown in this table, the catalysts are designated according to their Fe content (Fe-Z(0.2) for Fe-ZSM-5 prepared by ILIE, with 0.2 wt% iron). With a decreasing amount of iron used in the preparation, the iron content of the resulting samples also decreases. The iron content ranges from 1.2 to 0.2 wt%, and for the parent Na-ZSM-5-sample an iron impurity of 500 ppm was found.

During the EPR study, a weak V(IV) impurity signal was seen in some of the samples in the uncalcined state, which disappeared after calcinations. An ICP analysis of Fe-Z(0.2) resulted in a V content of about 200 ppm, and the EPR spectra did not indicate a significant increase of intensity with growing Fe content. The vanadium obviously originated from an impurity in the iron used because it was not present in repetitive preparations with a different iron source. Since the catalytic results of samples without a V EPR signal did not differ significantly from those with V impurity (which are presented here), it is clear that the catalytic behavior reported arises from the Fe species, not from the V impurity. This should have been expected for hydrocarbon-SCR, where vanadium is known to be of poor activity, whereas a considerable activity of zeolite-supported VO^{2+} ions for NH_3-SCR has been described earlier [37,38]. Apparently, however, the concentration of VO^{2+} is too low, or it is converted into inactive intra-zeolite V(V) sites [38] during the severe calcination step, so that a significant contribution from VO^{2+} could not be detected in NH_3-SCR as well.

N_2 physisorption data are also listed in Table 1. In the case of sample Fe-Z(0.2) the micropore volume does not significantly decrease in comparison with the parent Na-ZSM-5. With Fe-Z(1.2), however, a significant decrease from the initial 0.15 $cm^3\,g^{-1}$ to 0.12 $cm^3\,g^{-1}$ is observed.

3.2. Catalysis

Fig. 1a shows the temperature dependence of the NO conversions obtained in isobutane-SCR with the Fe-ZSM-5 catalysts prepared by the ILIE technique at 42,000 h^{-1} (conditions: set A-isobutane). With increasing reaction temperature, the NO conversions increase in all cases and pass through maxima. With growing iron content of the cata-

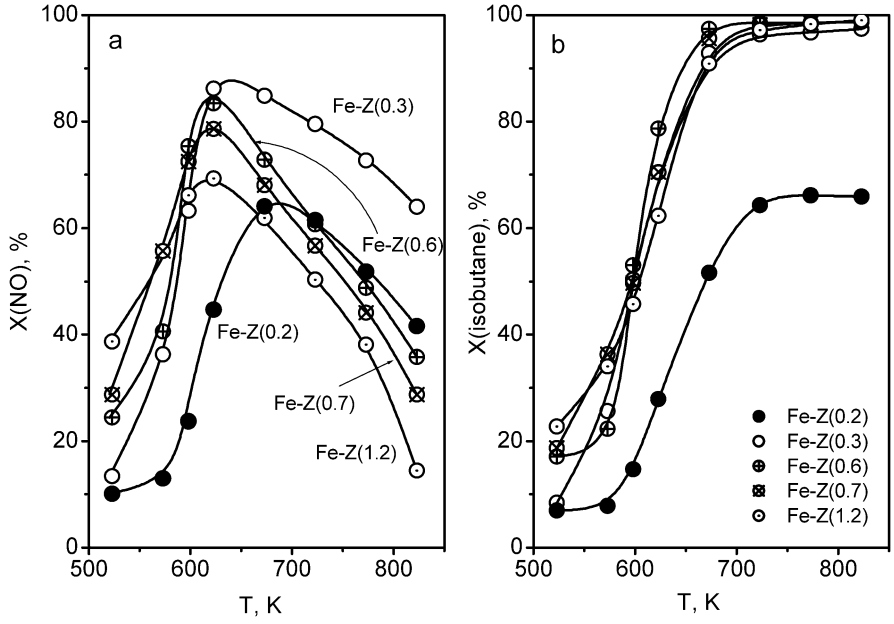

Fig. 1. SCR of NO with isobutane over Fe-ZSM-5 prepared by improved liquid ion exchange (ILIE). 2000 ppm NO, 2000 ppm isobutane, 3% O_2, 42,000 h^{-1}, (a) NO conversion; (b) isobutane conversion.

lysts, the NO conversion at the lowest reaction temperature (523 K) increases strongly (from 10 to almost 40%). The conversion maximum is shifted to lower temperatures, from ∼ 680 K (sample Fe-Z(0.2)) to ∼ 620 K (sample Fe-Z(1.2)). At the same time, the peak NO conversions achieved go through a maximum, ranging from 65% Fe-Z(0.2) via 86% Fe-Z(0.3), which is the highest NO conversion observed, to 69% Fe-Z(1.2). Remarkably, at temperatures above the conversion maxima ($T > 623$ K), a decreasing iron content leads to an increasing NO conversion (with the exception of ILIE-0.2), whereas at temperatures below the conversion maxima ($T < 573$ K) the trend is the opposite. In Fig. 1b the corresponding isobutane conversions can be found. Here, all samples, except for sample Fe-Z(0.2), show rather similar behavior. Remarkably, in the low-temperature range the NO conversions exceed the isobutane conversions at high Fe content, whereas they are about equal at low Fe content. All catalysts but Fe-Z(0.2) achieve a 50% isobutane conversion at ca. 600 K, where the NO conversions range 73–75% (Fe-Z(0.6), Fe-Z(0.7)) via 66% (Fe-Z(1.2)) to 63% (Fe-Z(0.3)). At temperatures higher than 670 K, the isobutane conversions exceed 90% and stay almost constant with a further temperature increase. Sample Fe-Z(0.2) shows lower isobutane conversions over the whole temperature range, with a maximum conversion of only slightly more than 65%.

Fig. 2 demonstrates that the ILIE series fills in the gap between the two types of Fe-ZSM-5 catalysts studied in our groups earlier [13,24,26,29]: those prepared by chemical vapor deposition of $FeCl_3$ into H-ZSM-5 (Fe-Z(CVD)) and by the mechanochemical route described in [26] (Fe-Z(MR)). With the smaller GHSV of condition set B-isobutane (which includes simultaneous decreases in the NO and isobutane concentration), the temperature of the NO conversion peak shifts slightly to lower values as expected, but, with the exception of Fe-Z(0.2), the peak NO conversion does not increase but decreases slightly. At the same time, the width of the selective temperature region is smaller under the conditions of set B, again with the exception of Fe-Z(0.2), which is the only sample that behaves more favorably under these conditions than under set A. From Fig. 2, from which two members of the ILIE series are omitted for the sake of clarity, it can be seen that Fe-Z(0.2) is similar to the MR sample, which also includes the unfavorable response of the latter upon application of set B conditions [39], whereas Fe-Z(0.7) (and Fe-Z(1.2), which is almost identical under these conditions) behaves like the CVD catalyst, again including the response to the change in reaction conditions [13].

Fig. 3a shows the temperature dependence of the NO conversions with the reductant ammonia at 750,000 h^{-1} (conditions: set A-NH_3). Here the sample with the highest Fe loading (Fe-Z(1.2)) shows a maximum behavior, as with the isobutane reductant. With the NH_3 reductant, however, the decrease after the conversion maximum is much less pronounced and the conversion maxima are found at higher temperatures ($T > 773$ K). The best catalysts compete favorably with the $V_2O_5/WO_3/TiO_2$ Eurocat [40], which has

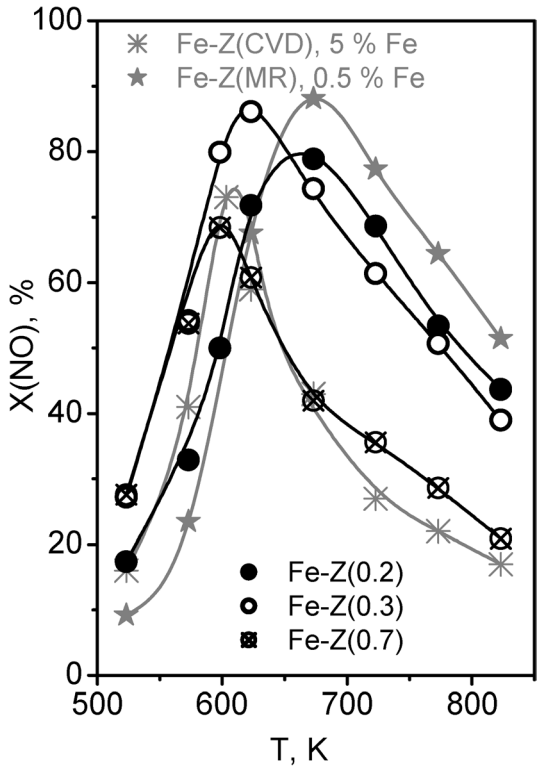

Fig. 2. SCR of NO with isobutane over Fe-ZSM-5. Comparison of preparation techniques: mechanochemical route according to [26] (Fe-Z(MR)), CVD of $FeCl_3$ into H-ZSM-5 (Fe-Z(CVD)), sample labeled A(CVD, W1, C5) in [13,24], and ILIE. 1000 ppm NO, 1000 ppm isobutane, 2% O_2, 30,000 h^{-1}.

been studied as a reference. At low iron content (Fe-Z(0.3) and Fe-Z(0.2)), the NO conversions increase monotonously with temperature. The NH_3 conversions are given in Fig. 3b, where the data of Fe-Z(CVD) and Fe-Z(MR) have been omitted; the curves for the former resemble that of Fe-Z(1.2), whereas for the latter the NH_3 conversions equal the NO conversions in the limits of experimental error. At low reaction temperatures, this is also true for all catalysts prepared by ILIE. At higher temperatures, the ammonia conversion goes on increasing slightly (up to values of about 95% with Fe-Z(1.2) in the range where the NO conversion starts to decrease with catalysts of higher Fe content). Hence, these catalysts oxidize ammonia at high temperatures, to an extent increasing with the Fe content. For Fe-Z(0.3) and Fe-Z(0.2), however, NO and NH_3 conversions are equal over the whole temperature range; that is, the ammonia oxidation activity of these catalysts is very small.

In Fig. 4, NO conversions obtained with isobutane and with ammonia are compared under identical conditions (set B) for some of the catalysts. As expected, the 25-fold decrease in the GHSV leads to significant downward shifts of the light-off temperature for NH_3-SCR. With Fe-Z(1.2), NO conversions around 40% are achieved at a temperature as low as 423 K. The NO conversions with isobutane (given as gray curves) always remain below those with NH_3;

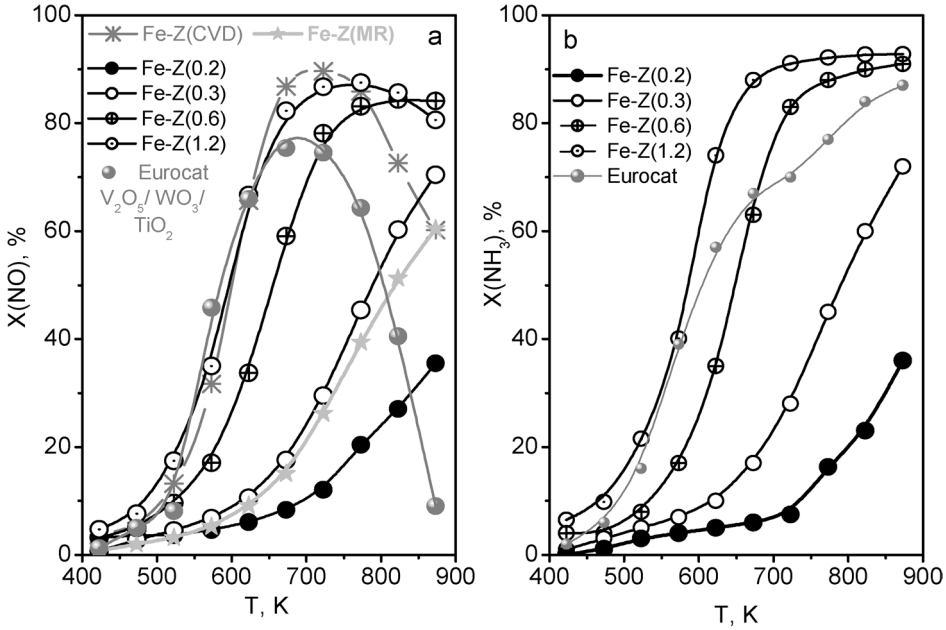

Fig. 3. SCR of NO with NH_3 over Fe-ZSM-5. Comparison of preparation techniques and relation to the $V_2O_5/WO_3/TiO_2$ system represented by the $V_2O_5/WO_3/TiO_2$ Eurocat [40]. 1000 ppm NO, 1000 ppm NH_3, 2% O_2, 750,000 h^{-1}. (a) NO conversion; (b) NH_3 conversion.

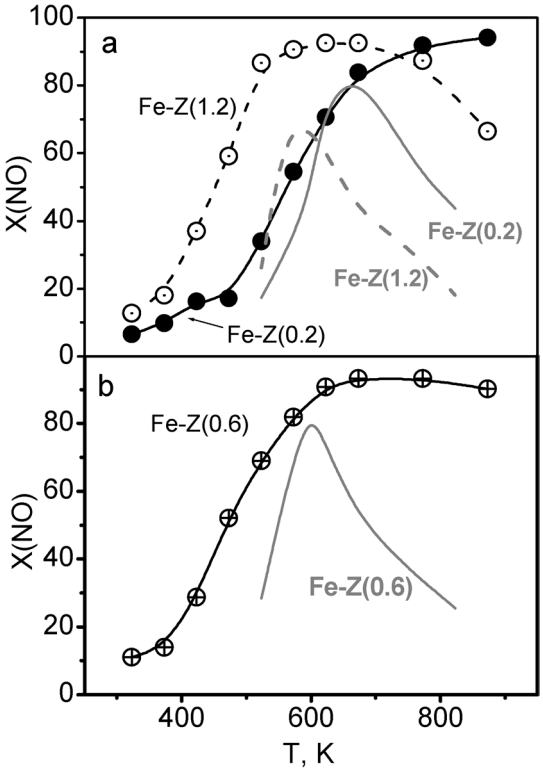

Fig. 4. Comparison of NO conversions over Fe-ZSM-5 with isobutane and NH_3 reductants. 1000 ppm NO, 1000 ppm isobutane (or NH_3), 2% O_2, 30,000 h^{-1}, black curves with data points for NH_3 reductant, grey curves (from Fig. 2) for isobutane reductant: (a) Fe-Z(0.2) and Fe-Z(1.2); (b) Fe-Z(0.6).

however, for the catalysts with lower Fe content, the conversions achieved are quite close in an intermediate temperature range around 573–673 K.

3.3. H_2-TPR

In Fig. 5, the H_2-TPR profile of sample Fe-Z(1.2) is compared with the profiles of reference samples: mechanical mixtures of α-Fe_2O_3 and γ-Fe_2O_3 with H-ZSM-5 (5 wt% Fe) and with Fe-Z(CVD). The hydrogen consumption is related to the iron content of the samples. The profiles of the mechanical mixtures show the well-known shape with a small low-temperature peak and a much more intense high-temperature peak, which are usually attributed to the reduction sequence $Fe_2O_3 \rightarrow Fe_3O_4 \rightarrow Fe(0)$. In comparison with the α-oxide sample, both peaks of the γ-oxide sample are shifted to higher temperatures (~ 650 K $\rightarrow \sim 690$ K; ~ 830 K $\rightarrow \sim 945$ K). It is not clear whether these temperature shifts arise from structural differences, as the reduction kinetic of iron oxides is also influenced by particle size, morphology, defect density, etc. [41]. As expected, integration of the TPR profiles gives H/Fe ratios of 3.0. The profile of the CVD sample is much more complicated than those of the iron oxides, which indicates a highly heterogeneous species distribution. Sample Fe-Z(1.2), however, exhibits a much simpler H_2 consumption curve with only two peaks in the region of the low-temperature peak of the reference oxides. At the same time, the H/Fe ratio observed with this sample (2.3) clearly exceeds the value of 1 expected for a reduction $Fe^{3+} \rightarrow Fe^{2+}$ and is close to the H/Fe ratio of the CVD catalyst.

3.4. XANES

Fig. 6 shows the near-edge region of the normalized X-ray absorption spectra for the prepared samples and those for α-Fe_2O_3 and γ-Fe_2O_3 as reference materials and the ref-

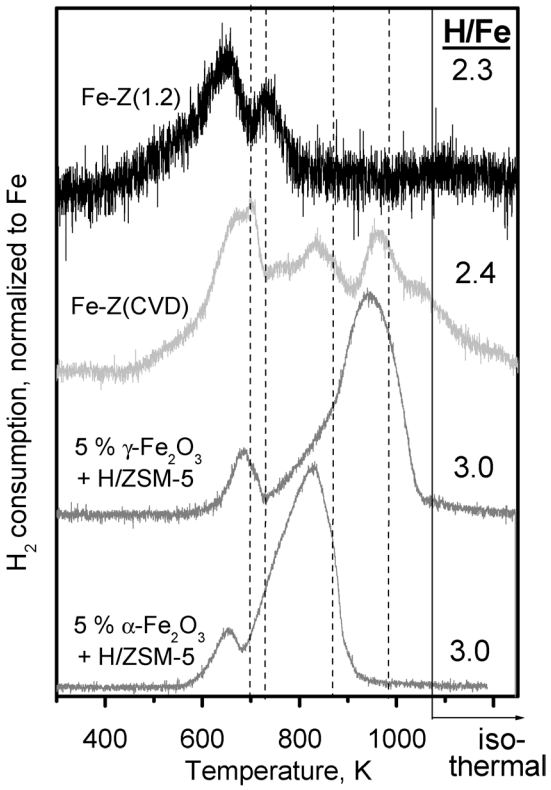

Fig. 5. TPR traces of a catalyst prepared by ILIE, compared with reference samples: Fe-Z(CVD), α-Fe_2O_3 and γ-Fe_2O_3 mixed with H-ZSM-5.

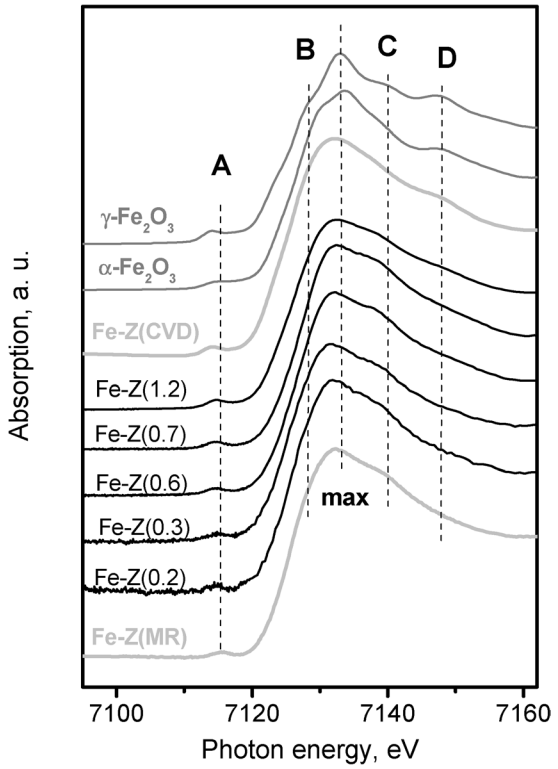

Fig. 6. Fe *K* XANES of Fe-ZSM-5 prepared by ILIE, compared with reference spectra: α-Fe_2O_3 and γ-Fe_2O_3, Fe-Z(CVD), and Fe-Z(MR). Spectrum of Fe-Z(0.2) measured in fluorescence mode, remaining spectra in transmission mode.

erence catalysts Fe-Z(CVD) and Fe-Z(MR) for comparison. The edge positions of all samples are quite similar, indicating that the oxidation state of iron in the samples under study is predominantly +3, as in the reference oxides. In all spectra a pre-edge peak (A) is observed. This peak arises from a $1s \rightarrow 3d$ transition, which is forbidden for coordination geometries with an inversion center. Therefore, the origin of this signal could be iron in tetrahedral or in distorted octahedral coordination. The spectra of all ILIE samples are quite similar, but there are significant differences to the reference samples in the edge shape and the post-edge region. On the one hand, the increase in the absorption coefficient in the step is steeper with the zeolite-supported Fe species than with γ-Fe_2O_3, and there is no low-energy shoulder as in the latter (labeled B). The maximum of the absorption coefficient is earlier than with both reference oxides, which can be, however, a consequence of insufficient resolution between the maximum and a low-energy shoulder very close to it, as in the case of α-Fe_2O_3. A high-energy shoulder at the maximum (labeled C) is very pronounced in all Fe-ZSM-5 samples, whereas it has lower intensity in the spectra of the reference oxides. A maximum at ca. 7150 eV (D), which is observed in the spectra of both reference oxides, may be identified as a weak feature with Fe-Z(1.2), but it is absent in the remaining samples. Therefore, the XANES does not indicate the presence of iron in a well-defined short-range order typical of one of the reference oxides. The shape of the pre-edge peak is closer to that observed with γ-Fe_2O_3 containing Fe ions in both octahedral and tetrahedral coordinations, which suggests that both coordinations may be present in the zeolite samples as well. The shape of the step and of the post-edge region resembles the spectrum of α-Fe_2O_3 rather than that of γ-Fe_2O_3.

3.5. EXAFS

Fig. 7 presents the absolute part of the Fourier-transformed k^2-weighted spectra for the calcined Fe-ZSM-5 samples under study and α-Fe_2O_3 and, for comparison, the spectra for Fe-Z(CVD) and Fe-Z(MR). All spectra, including that for the reference oxide, show a signal at distances smaller than 2 Å (uncorrected), which is attributed to O scatterers. The intensities of this scattering feature are quite similar in all samples, whereas height and width vary to some extent. No long-range order above 4 Å (uncorrected) can be detected in any of the samples, which is normally taken to indicate the absence of large oxide particles (see, however, [13,24] and below). The scattering events between 2 and 3.5 Å, which are very intense in α-Fe_2O_3 and arise mostly from Fe neighbors there, are also of low intensity in the zeolite samples. A qualitative comparison of this region shows that in most samples of the ILIE series, the extent of Fe aggregation should be smaller than in the CVD sample. There is some resemblance in the spectra for the latter and for Fe-

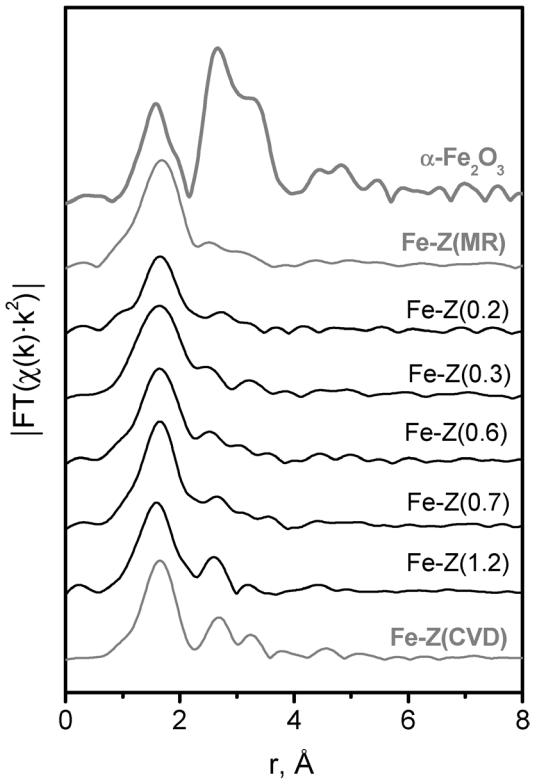

Fig. 7. EXAFS spectra (modulus of the Fourier-transformed, k^2-weighted spectra) of Fe-ZSM-5 prepared by ILIE, compared with reference spectra: α-Fe_2O_3, Fe-Z(CVD), and Fe-Z(MR). Spectrum of Fe-Z(0.2) measured in fluorescence mode, remaining spectra in transmission mode.

Table 2
Fit results in comparison to crystallographic data of α-Fe_2O_3

No.	Element	Fit results ($R = 8.3\%$)			Crystallographic data	
		R (Å)	CN	σ^2 (10^{-3} Å^{-2})/ ΔE_0 (eV)	R (Å)	CN
1	O	1.99	2.8	4.5/25.4	1.9457	3
2	O	2.16	3.0	6.9/26.3	2.1162	3
3	Fe	2.96	5.3	6.5/16.1	2.9004	4
4	Fe	3.37	3.8	5.4/16.3	3.3642	3
5	Fe	3.69	2.9	2.1/16.5	3.7053	6
6	O	3.75	1.8	1.0/25.9	3.7857	3

Fit for 2.5 Å^{-1} $< k <$ 14 Å^{-1}, and an R window of $\Delta R = 3.16$ Å.

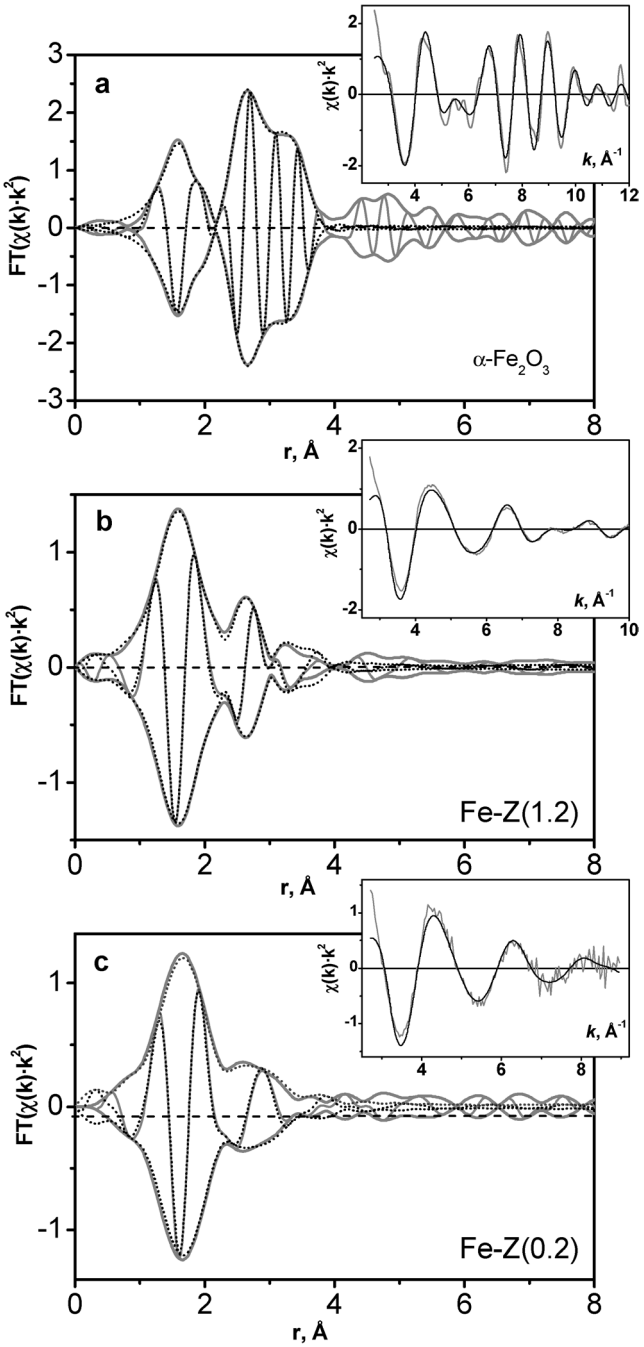

Fig. 8. Examples for model fits of EXAFS spectra. (a) α-Fe_2O_3; for model parameters see Table 2; (b) Fe-Z(1.2); (c) Fe-Z(0.2); for model parameters see Table 3.

Z(1.2), but the scattering feature at 3.4 Å (uncorrected) is much less intense in the ILIE sample.

To confirm the applicability of scattering functions (amplitudes, phases) supplied by the FEFF8.10 code, it is necessary to test them by fitting a reference system. Fig. 8 and Table 2 report results of such a test, which was performed with α-Fe_2O_3. It should be noted that the Fe(III) oxides are unfavorable references because they contain a considerable number of closely related neighboring shells (cf. Table 2) and involve several multiple scattering paths, which have been neglected in the fit reported here. Even so, a large number of free parameters might imply that the models fail to meet the Nyqvist criterion that determines the number of free parameters to be sensibly fitted from a given spectral range in k and R space (actual values given in Tables 2 and 3). It should be noted, however, that the constraints used (see Experimental section) limit the number of free parameters to acceptable values, maybe with the exception of the full models for Fe-Z(0.3) and Fe-Z(0.2).

The fit of the second coordination sphere as summarized in Fig. 8a and Table 2 is quite acceptable and shows that the scattering functions provided by FEFF8.10 are reliable for

Table 3
Fitting results for the Fe-ZSM-5 samples (6-shell model)

Sample	No.	Element	R (Å)	CN	σ^2 (10^{-3}Å^{-2})/ ΔE_0 (eV)
Fe-Z(1.2)[a]	1	O	2.00	3.5	7.7/23.5
$R = 11.2\%$	2	O	2.19	0.9	1.7/23.0
	3	Fe	3.02	1.1	7.7/22.3
	4	Fe	3.51	1.1	2.9/22.3
	5	Fe	3.68	1.2	1.3/23.3
	6	O	3.77	6.4	1.3/22.5
Fe-Z(0.7)[b]	1	O	2.03	4.8	9.7/24.9
$R = 8.6\%$	2	O	2.26	0.6	1.0/24.8
	3	Fe	3.03	0.9	10.4/24.4
	4	Fe	3.58	1.0	1.5/24.4
	5	Fe	3.73	1.2	1.0/25.4
	6	O	3.82	7.4	10.0/23.9
Fe-Z(0.6)[b]	1	O	2.04	4.4	8.8/25.1
$R = 9.1\%$	2	O	2.25	1.0	1.0/24.5
	3	Fe	3.02	0.9	8.6/24.4
	4	Fe	3.60	1.1	1.8/24.4
	5	Fe	3.75	1.3	1.3/25.4
	6	O	3.83	6.4	5.7/24.1
Fe-Z(0.3)[c]	1	O	2.06	4.5	16.0/22.1
$R = 12.8\%$	2	O	2.23	0.2	2.4/23.0
	3	Fe	3.03	0.7	8.8/24.8
	4	Fe	3.53	0.3	1.0/24.9
	5	Fe	3.71	0.8	1.0/25.7
	6	O	3.82	4.4	5.3/22.0
Fe-Z(0.2)[d]	1	O	2.08	3.4	9.3/22.7
$R = 12.2\%$	2	O	2.30	0.5	6.3/21.8
	3	Fe	3.13	0.9	16.2/24.5
	4	Fe	3.59	0.4	9.9/24.5
	5	Fe	3.79	1.0	6.9/25.4
	6	O	3.82	4.8	16.7/21.7

[a] 2.71 Å^{-1} $< k <$ 12.0 Å^{-1}, $\Delta R = 3.41$ Å.
[b] 2.71 Å^{-1} $< k <$ 11.5 Å^{-1}, $\Delta R = 3.39$ Å.
[c] 2.71 Å^{-1} $< k <$ 10.0 Å^{-1}, $\Delta R = 3.08$ Å.
[d] 2.71 Å^{-1} $< k <$ 10.0 Å^{-1}, $\Delta R = 2.83$ Å.

this system. At the same time, the comparison with the crystallographic data indicates which systematic error has to be expected with the simplified model employed. Apart from some deviations in the distances of the closely neighboring O shells, there are, in particular, errors in the Fe coordination numbers (CNs). The CNs of shells 3 and 4 are overestimated by ca. 30%, whereas those of shell 5 and the last (oxygen) shell are seriously underestimated, which may have been caused by a rather small impact of these scattering events on the total signal of the second coordination sphere.

Figs. 8b and c exemplify the application of this model to samples Fe-Z(1.2) and Fe-Z(0.2). Fit results for all samples are listed in Table 3. In all cases, the sum of the coordination numbers of the first two O shells is between 4 and 6, which indicates the presence of octahedrally and tetrahedrally coordinated iron. The sum of the coordination numbers of the iron shells, which is 13 in α-Fe_2O_3, decreases with decreasing iron content of the zeolite samples from 3.4 (sample Fe-Z(1.2)) to 2.3 (sample Fe-Z(0.2)). As for the interatomic distances, there is no perfect coincidence with those in α-Fe_2O_3 already in Fe-Z(1.2), and a tendency of the coordination shells to move to even higher distances is observed with decreasing iron content of the samples. Obviously, the short-range order of the aggregates, while reminiscent of that of α-Fe_2O_3 in Fe-Z(1.2), differs more and more from this oxide with decreasing Fe content. The high Debye–Waller factor of the first iron shell indicates a large degree of disorder in the particles or a superposition of different types of short-range order, as suggested already by the XANES and found earlier in Fe-Z(CVD) [13]. The increase in the goodness-of-fit-parameter has analogous implications.

Table 4
Fitting results for the Fe-ZSM-5 samples (4-shell model)

Sample	No.	Element	R (Å)	CN	σ^2 (10^{-3}Å^{-2})/ ΔE_0 (eV)
Fe-Z(1.2)[a]	1	O	2.01	3.5	6.7/26.3
$R = 12.9\%$	2	O	2.22	1.2	1.2/26.6
	3	Fe	3.06	7.4	23.0/22.5
	4	Fe	3.34	6.8	24.1/23.4
Fe-Z(0.2)[b]	1	O	2.07	2.5	2.2/26.6
$R = 11.7\%$	2	O	2.27	1.6	1.0/27.6
	3	Fe	3.00	2.1	12.3/20.0
	4	Fe	3.22	5.4	21.5/19.6

[a] 2.71 Å^{-1} $< k <$ 12.0 Å^{-1}, $\Delta R = 3.41$ Å.
[b] 2.71 Å^{-1} $< k <$ 10.0 Å^{-1}, $\Delta R = 2.83$ Å.

The low intensity of the scattering events above 3 Å (uncorrected) prompted us to also try models with a lower number of Fe neighbors, which would meet the Nyqvist criterion also at low Fe content. Models with only one Fe neighbor did not provide satisfactory fits at all; two examples with two Fe shells, which have also been tried to test the suitability of a γ-Fe_2O_3 short-range order in our case, are summarized in Table 4. It appears that these models are inappropriate as well, because they result in unrealistically high iron CNs and Debye–Waller factors.

In summary, our XAFS results imply that ILIE produces samples with a lower degree of aggregation than CVD of $FeCl_3$ into H-ZSM-5, with decreasing cluster content at smaller Fe content. At high Fe content (1.2 wt%), there is some structural similarity of the clustered phase to α-Fe_2O_3 (and a definite dissimilarity compared with γ-Fe_2O_3, which has a first Fe–O shell below 1.9 Å and only two Fe–Fe shells in the second coordination sphere); however, significant deviations (or the presence of an additional clustered structure) are obvious and become more pronounced at lower Fe contents. Even in the material with a higher degree of aggregation, no order beyond 3.5 Å (uncorrected) was detected.

3.6. UV–vis

UV–vis spectra of Fe-ZSM-5 catalysts prepared by ILIE and calcined in air are displayed in Figs. 9a–e, where spectra of reference samples are also given (Figs. 9f–h). The spectral shapes, which vary strongly with the iron content, may be represented by sub-bands, as indicated in the fig-

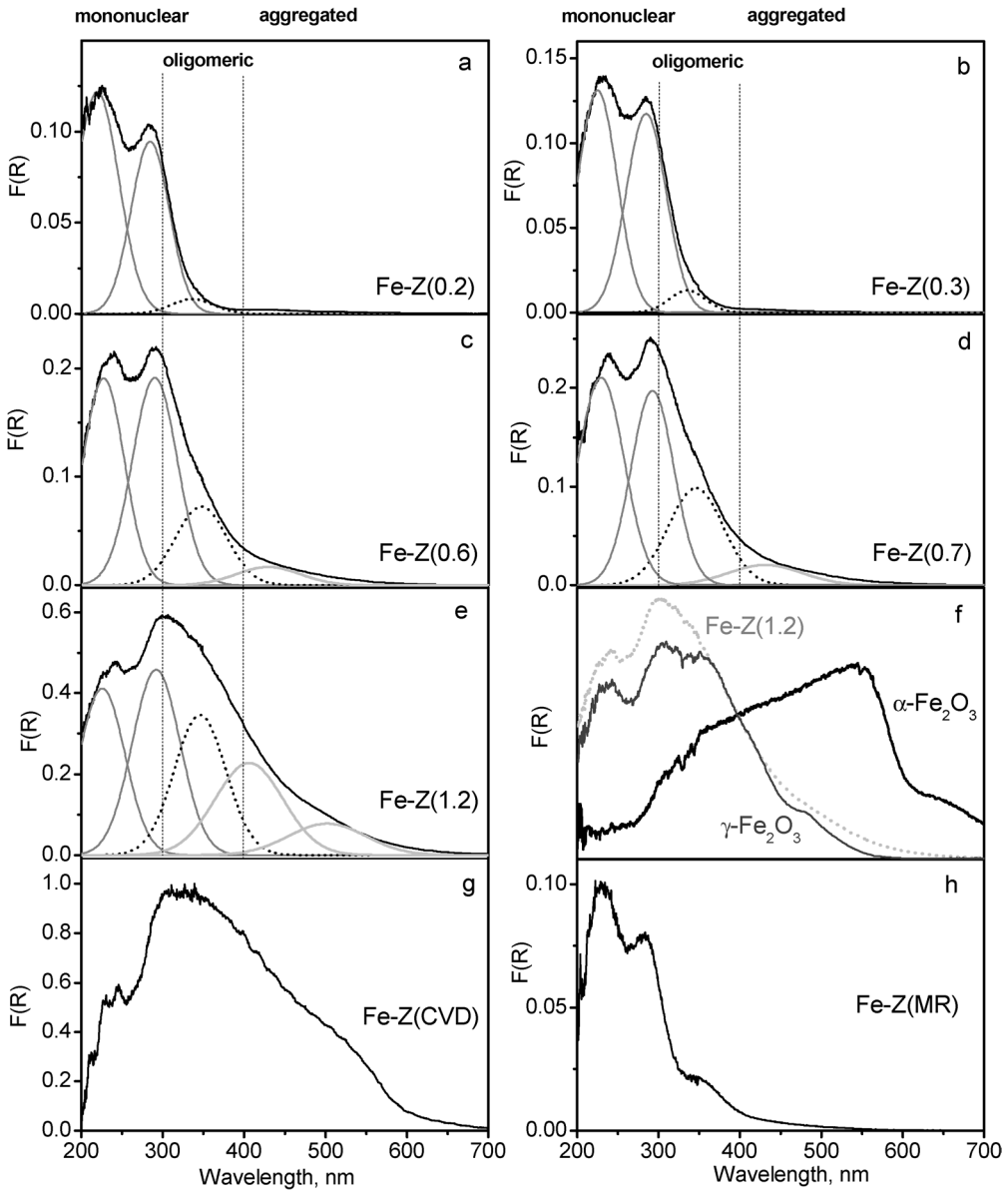

Fig. 9. UV–vis spectra of Fe-ZSM-5 prepared by ILIE, after calcination in air at 823 K, compared with reference spectra. (a) Fe-Z(0.2); (b) Fe-Z(0.3); (c) Fe-Z(0.6); (d) Fe-Z(0.7); (e) Fe-Z(1.2); (f) α-Fe_2O_3 and γ-Fe_2O_3; (g) Fe-Z(CVD); (h) Fe-Z(MR). In panel (f), the spectrum of Fe-Z(1.2) is added in gray, enlarged to include the γ-Fe_2O_3 spectrum completely in the range assigned to large aggregates ($\lambda > 400$ nm). This comparison shows that in Fe.Z(1.2) the intensity at < 300 nm (isolated sites) cannot be accounted for completely by contributions from aggregates even in the most unfavorable case.

ures (for numerical results see Table 5). At low Fe content, there is hardly any signal above 400 nm, and 95% of the spectral intensity is accounted for by sub-bands centered at $\lambda < 300$ nm (Table 5). With increasing Fe content (Fe-Z(0.6), Fe-Z(0.7)), the spectrum becomes broader, but ca. 95% of the spectral intensity is still covered by bands centered below 400 nm. Only the spectrum of Fe-Z(1.2) extends significantly to wavelengths above 400 nm.

The assignment of the sub-bands has been discussed in some detail in [24,28] and is based on earlier proposals made in [42]. We ascribe the bands at ~ 220 nm and ~ 285 nm to $Fe^{3+} \leftarrow O$ charge transfer bands of isolated Fe ions in tetrahedral and octahedral coordination, respectively ($t_1 \rightarrow$

Table 5
Numerical analysis of UV–vis spectra of Fe-ZSM-5 catalysts (Fig. 9). Percentage of the sub-bands ($I_1 - \lambda < 300$ nm, $I_2 - 300 < \lambda < 400$ nm, $I_3 - \lambda > 400$ nm) and wt% Fe of the corresponding species (see text)

Catalyst	Fe_1[a]		Fe_2[b]		Fe_3[c]		Total Fe
	I_1 (%)	(wt%)	I_2 (%)	(wt%)	I_3 (%)	(wt%)	(wt%)
Fe-Z(0.2)	95.7	0.19	4.3	0.01	–	–	0.2
Fe-Z(0.3)	95.0	0.28_5	5.0	0.01_5	–	–	0.3
Fe-Z(0.6)	76.2	0.46	18.5	0.11	5.3	0.03	0.6
Fe-Z(0.7)	70.7	0.49_5	22.9	0.16	6.4	0.04_5	0.7
Fe-Z(1.2)	48.6	0.58	23.4	0.28	28.0	0.34	1.2

[a] Isolated Fe^{3+} in tetrahedral and higher coordination.
[b] Oligomeric $Fe_x{}^{3+}O_y$ clusters.
[c] Large Fe_2O_3 particles.

$t_2/t_1 \rightarrow e$ transitions unresolved); the band at ~ 350 nm to oligomeric clusters; and sub-bands above 400 nm to large particles. From the intensity of the sub-bands and the relative percentage, and by multiplication with the total Fe content, the amount of each kind of Fe species has been derived (Table 5). This analysis neglects the wavelength dependence of the absorption coefficient, which is not known for this system. However, since the variation in the absorption coefficient may be expected to be smooth and not erratic, the values obtained may be considered a meaningful approximation, possibly superimposed by a moderate systematic deviation that does not affect the conclusions of the present work. Indeed, absorption coefficients determined for Co^{2+} ions at different positions in pentasil zeolites were found to differ only marginally [43]. According to Table 5, ca. 95% of the iron is mononuclear in Fe-Z(0.2) and Fe-Z(0.3). With increasing Fe content, the percentage of isolated sites decreases, but because of the increased Fe content of the samples, the absolute amount of isolated iron species in the catalysts goes on increasing and levels off above 1% Fe.

In samples with significant particle content (Fe-Z(1.2)), there is some uncertainty regarding the actual percentage of isolated sites because contributions of the particles in the $\lambda < 300$ nm wavelength region cannot be completely ruled out. Fig. 9f shows UV–vis spectra of possible references for the particles α-Fe_2O_3 and γ-Fe_2O_3. Whereas the former does not contribute below 300 nm, the latter does. The EXAFS results, although indicating in general a high disorder in the aggregated species (see also Discussion section), give some preference to the α-Fe_2O_3 short-range order, however with strong distortions or coexistence of a different type of short-range order. However, even if all intensity found for Fe-Z(1.2) at 400 nm and above was assigned to well-crystallized γ-Fe_2O_3, there would remain a significant excess intensity over the γ-Fe_2O_3 contribution below 300 nm (see Fig. 9f, where the spectrum of Fe-Z(1.2) has been scaled to match that of γ-Fe_2O_3 in the region around 400 nm), which proves the presence of isolated sites in significant quantities also in Fe-Z(1.2). While we consider the assumption of an ordered γ-Fe_2O_3 particulate phase as highly unrealistic (vide supra), it may be safer to consider the 0.5 wt% of isolated Fe^{3+} species in Fe-Z(1.2) (Table 5) as an upper limit.

3.7. TEM

In Fig. 10, TEM micrographs of sample Fe-Z(1.2) are compared with those of Fe-Z(CVD). In both samples, large iron oxide aggregates can be clearly detected. They coexist with much smaller particles (see, e.g., Fig. 10, lower left panel), which are probably intra-zeolite. Generally, the size of the big aggregates is larger in Fe-Z(CVD) than in Fe-Z(1.2); typical sizes are between 20 and 50 nm in the former and between 5 and 20 nm in the latter. Their surfaces are usually curved. Only in Fe-Z(CVD) were some (rare) examples of well-crystalline oxide aggregates with sharp edges found on the external zeolite surface (Fig. 10, marked by arrows in upper left panel). The location of the aggregates with

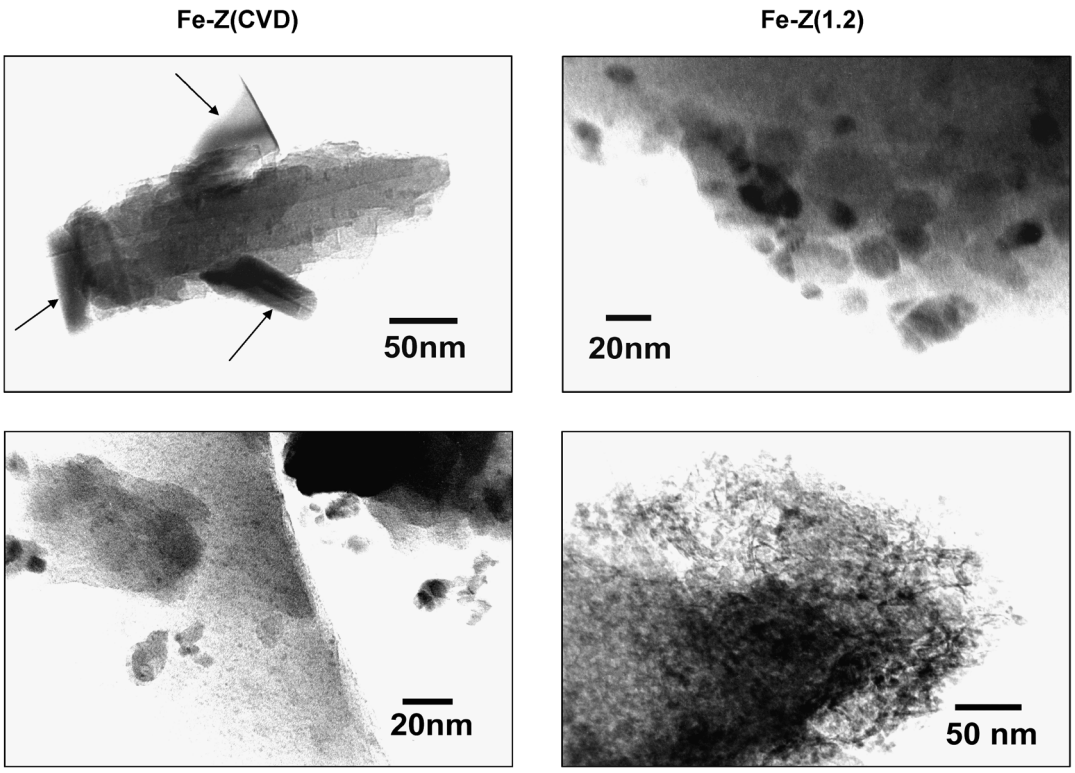

Fig. 10. TEM micrographs of Fe-Z(CVD) and Fe-Z(1.2).

curved boundaries is less clear. Whereas extra-zeolite location is likely with some of them, others seem to be covered by a layer of light matter. On the whole, a broad particle size distribution is seen in both samples, with an upper end at much higher sizes for Fe-Z(CVD).

During the measurements, a strong perturbation of the electromagnetic lens field, which had to be corrected to obtain high-quality micrographs, was observed for sample Fe-Z(1.2) but not for Fe-Z(CVD). This is a hint for a higher net magnetic moment of sample Fe-Z(1.2).

EDX measurements of the zeolite crystals in sample Fe-Z(1.2) at positions free of Fe_2O_3 particles always showed the presence of iron. This suggests that inside the pore system there is a rather homogeneous distribution of Fe. For Fe-Z(CVD), areas free of Fe_2O_3 were difficult to find, because of the rather homogeneous distribution of very small particles (Fig. 10, lower left panel). In certain areas of sample Fe-Z(1.2) a porous cloudy structure was detected that contained, in addition to Si and Al, about 30% Fe (Fig. 10, lower right panel). This species was probably formed by partial destruction of the zeolite lattice due to the long-term treatment in HCl solution. However, these amorphous structures were clearly a minority feature.

3.8. EPR

In Fig. 11, ex situ EPR spectra for calcined Fe-ZSM-5 prepared by ILIE are presented. In Figs. 11a and b, spectra recorded at 77 and 298 K are compared. Several signals known from earlier studies [24,28] can be distinguished. Signals at $g \approx 4.3$ and $g \approx 6$ (which is weak under ambient conditions because of the influence of adsorbed water, but more pronounced at higher temperatures (Figs. 11c, d)) have been assigned to isolated Fe^{3+} ions in tetrahedral coordination and in environments with more neighboring oxygen ions (5 or 6), respectively. In addition, a narrow and a broad signal at $g \approx 2$ can be discerned.

In samples Fe-Z(0.2) and Fe-Z(0.3) the $g \approx 2$ EPR signal is assigned to isolated Fe^{3+} ions in a highly symmetric environment (Fig. 11a). This is also consistent with the fact that the line intensity increases markedly with cooling to 77 K, which is typical for pure paramagnetic behavior according to the Curie–Weiss law. It is also in agreement with UV–vis results that indicate the presence of almost exclusively isolated Fe species (Figs. 9a and b). In samples with 0.6 and 0.7% Fe, for which UV–vis spectra indicate the presence of a certain amount of oligomers and even some Fe_2O_3 nanoparticles (bands above 300 and 400 nm in Figs. 9c and d), a broad line with a low field maximum around 2350 G at 298 K is superimposed on the narrow signal at $g \approx 2$ (Figs. 11a, b). In sample Fe-Z(1.2), where UV–vis showed a pronounced trend toward formation of oxide particles, which according to TEM have a size of several nanometers (Figs. 9e, 10), the linewidth of the broad signal is even larger, shifting the low field maximum to about 880 G, whereas the narrow line, though easily visible, does not increase with rising tem-

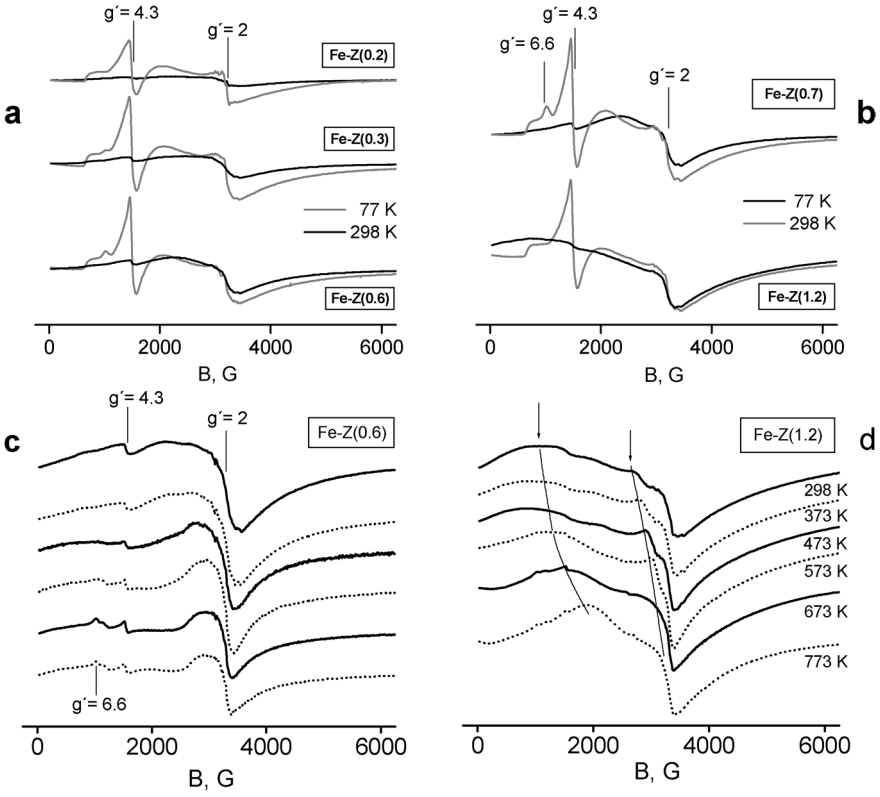

Fig. 11. EPR spectra of Fe-ZSM-5 prepared by ILIE. (a, b) comparison of spectra taken at 77 K and room temperature; (c, d) temperature dependence of the spectra of Fe-Z(0.6) (c) and Fe-Z(1.2) (d).

perature, which indicates a deviation from a paramagnetic (isolated) nature (Fig. 11b).

It was shown earlier that the temperature dependence of the signal intensity bears valuable information on the presence of magnetically coupled phases [24,44,45]. Whereas well-ordered crystalline α-Fe_2O_3 is antiferromagnetic below the Neel temperature $T_N = 960$ K and should therefore not be EPR-active, it has been shown that nanoparticles of α-Fe_2O_3 ($d \approx 3$ nm) do give rise to an EPR signal below T_N because of incomplete compensation of the spin moments [43]. At low temperature, these particles show ferrimagnetic behavior. In the EPR spectra, this is reflected by broad anisotropic signals, since the resulting magnetic moment vectors of the particles tend to align with the direction of the external magnetic field. With rising temperature, thermal fluctuations lead to the collapse of the ferrimagnetic order and the particles become superparamagnetic above the so-called blocking temperature. As a result, the EPR signal narrows and shifts toward $g \approx 2$ as the temperature increases [45]. It was also shown that the transition from the ferrimagnetic to the superparamagnetic state is shifted to higher temperatures as the particles become larger; that is, for a given temperature the EPR linewidth increases with the size of the magnetic particles. Thus, characteristic EPR spectra have been observed for samples with a certain distribution of Fe_2O_3 particle diameters, which consist of a superposition of a broad anisotropic and a narrow isotropic signal [46].

Against this background, temperature-dependent EPR measurements have been performed with samples Fe-Z(0.6) and Fe-Z(1.2) (Figs. 11c and d) as described earlier for Fe-Z(CVD) in [24] to gain more information about differences in the nature of the iron oxide aggegates. From Fig. 11c it can be seen that the signal at $g \approx 2$ for sample Fe-Z(0.6) narrows slightly and follows a Curie-like temperature dependence, which is typical for both isolated Fe^{3+} ions but also for oxide nanoparticles in the superparamagnetic state. UV–vis measurements (Fig. 9c) suggest that this sample is dominated by isolated Fe^{3+} ions with a small contribution of oligomers. Because of their location inside the pore system, these oligomers are assumed to consist of a few Fe atoms only, which is probably not enough to create superparamagnetic behavior. Therefore, the $g \approx 2$ signal in sample Fe-Z(0.6) has to be regarded as arising from both highly symmetric isolated Fe^{3+} species and small oligomers with weak dipolar coupling.

The EPR spectrum of sample Fe-Z(1.2) at 298 K is characterized by a very broad anisotropic line and two narrower features at $g \approx 2$ (Fig. 11d). The two broader lines narrow and are shifted to a higher resonance field with increasing temperature (marked with arrows). Based on the considerations above, these two signals can be assigned to ferrimagnetic/superparamagnetic Fe_2O_3 particles of different size, whereas the remaining narrow signal at $g \approx 2$ might be due to isolated and weakly interacting Fe^{3+} sites. In contrast to sample Fe-Z(1.2) prepared by ILIE, a huge, rather narrow signal appeared at $g \approx 2$ in Fe-Z(CVD) upon heating above 373 K [24]. The difference in the temperature dependence of the EPR signals of the two samples might be due to the difference in particle size, which is also detected by TEM (Fig. 10). In Fe-Z(CVD), particles larger than 50 nm are formed, whereas the particles are much smaller in Fe-Z(1.2). It is possible that the former are truly antiferromagnetic up to a temperature of about 400 K, and the latter change from ferrimagnetic to superparamagnetic at markedly lower temperatures. This would also explain why the observed perturbation of the electromagnetic lens field during TEM measurements was strong for sample Fe-Z(1.2) but negligible for Fe-Z(CVD).

4. Discussion

4.1. Structure of the Fe sites

The results of the spectroscopic investigation show that the improved liquid ion exchange technique gives access to samples that are structurally more homogeneous than those prepared by CVD of $FeCl_3$ into H-ZSM-5. On the other hand, it makes it possible to vary the site structure to include oligomeric and particulate moieties as present in the CVD-derived Fe-ZSM-5. At an iron content less than or equal to 0.3 wt%, ca. 95% of the iron is present in mononuclear sites. This conclusion is based mainly on the UV–vis data (Fig. 9, Table 5). It is confirmed, however, by the EPR results (Fig. 11a), where all signals observed with Fe-Z(0.2) and Fe-Z(0.3) could be assigned to isolated sites and exhibit paramagnetic behavior. The EXAFS results support this conclusion qualitatively with a very low sum coordination number of the neighboring Fe shells (1.8–2.4 in Fe-Z(0.3) and Fe-Z(0.2) vs 13 in α-Fe_2O_3). Such a low coordination number indicates either a very small average size of the aggregates or the coexistence of a small number of aggregates with an excess of isolated sites.

At 0.6–0.7 wt% Fe, coexistence of isolated and oligomeric moieties is found by UV–vis spectroscopy (Fig. 9, Table 5), and an increasing clustering tendency is supported by EXAFS, where the Fe sum coordination number increases above 3 (Table 3). The coexistence of isolated Fe^{3+} ions and weakly interacting Fe sites within oligomers of low nuclearity is also suggested by the temperature dependence of the EPR spectra (Fig. 11c). However, the missing ferrimagnetic/superparamagnetic behavior confirms that the formation of extended oxide particles does not take place at Fe contents of 0.6–0.7%. At an Fe content of 1.2%, the aggregation is obvious, not only from UV–vis and TEM measurements, but also from the EPR spectrum itself, the temperature dependence of which is typical for ferrimagnetic/superparamagnetic Fe_2O_3 nanoparticles (Fig. 11d).

Given the literature reports on conflicting results of different techniques regarding the size of the Fe oxide nanoparticles, a more detailed discussion of this question is of in-

terest. In the TEM micrographs, the difference in the particle sizes in Fe-Z(1.2) and Fe-Z(CVD) is shown directly (Fig. 10). The difference is also clearly indicated by the different temperature dependence of the EPR spectra (compare Fig. 11d with Fig. 2 in [24]), since the temperature series shows the antiferromagnetic/paramagnetic transition in Fe-Z(CVD) at a markedly higher temperature than with Fe-Z(1.2). The strong perturbation of the electromagnetic lens field during the TEM investigation of Fe-Z(1.2) (but not with Fe-Z(CVD)) gives an additional hint of a smaller particle size in the latter.

Differences in the particle size are also accounted for by the TPR results. Indeed, in the TPR trace of ILIE-1.2 (Fig. 5), there is much less intensity at high temperatures, which is usually assigned to aggregates (cf. spectra of reference oxides). The reduction degree achieved with Fe-Z(1.2) is well above $H/Fe = 1$, which would be expected for Fe^{3+} ions at cation positions. It is, in fact, comparable to that of Fe(CVD), indicating a similar amount of Fe in clusters, the size of which is smaller.

On the other hand, UV–vis seems to be insensitive in the range of sizes considered. The range of cluster sizes in which the absorption shifts from the 300–400 nm wavelength region to $\lambda > 400$ nm is unknown. Already in [24] it has been shown by comparison of temperature-dependent EPR data with UV–vis spectra that aggregates of strongly varying sizes give indistinguishable UV–vis bands above 400 nm. This is now confirmed by a comparison of the TEM micrographs, which show very different particle sizes for Fe-Z(1.2) and Fe-Z(CVD) (Fig. 10) with the respective UV–vis spectra (Figs. 9e and g), which are very similar despite the lower Fe content.

As observed already in [13] and confirmed in [25], EXAFS fails to indicate the very extended Fe oxide aggregates formed upon thermal stress in the Fe-ZSM-5 catalysts. The sum coordination number of the Fe shells does not increase significantly from Fe-Z(0.7) to Fe-Z(1.2) (Table 3), and it appears to be small, given the considerable extent of aggregation indicated by the UV–vis spectrum (Fig. 9) and the size of the particles shown in the TEM micrographs (Fig. 10). The difference in the EXAFS spectra between Fe-Z(1.2) and Fe-Z(CVD) (Fig. 7), in which very large aggregates were detected by Mössbauer and EPR spectroscopy [13,24] and now by TEM, consists just of smaller intensities of the scattering event at 3.3 Å (uncorrected) and of some doubtful features between 4 and 5 Å (uncorrected) in Fe-Z(1.2). This confirms, indeed, the lower extent of aggregation in Fe-Z(1.2), but it does not allow more detailed conclusions to be drawn, because of the obvious insensitivity of the method to the aggregates.

It has been discussed in [13,25] that the failure of EXFAS to detect these particles should be due to a high degree of disorder in them. Our TEM images (Fig. 10) confirm this view. In both samples studied, the majority of iron seen by TEM appears to be involved in large aggregates with curved surfaces and in very small intra-zeolite particles (Fig. 10, lower left and upper right panels). It has been demonstrated in [13] that EXFAS is able to detect long-range order in Fe oxide particles that are formed during solid-state ion exchange of an excess of $FeCl_3$ into H-ZSM-5 followed by calcinations without intermediate washing. These particles probably had never been intra-zeolite. Well-crystallized particles on the external zeolite surface are found also in Fe-Z(CVD) (Fig. 10, upper left panel), but they are very rare. Since aggregation is known to occur only upon washing and calcination in Fe-ZSM-5 prepared by CVD of $FeCl_3$ into H-ZSM-5 [13,24,39], these crystalline particles do not seem to be a result of incomplete distribution of the iron, but rather the final state of a migration process. This migration process transfers mononuclear iron species from intra- to extra-zeolite locations, with intermediate formation of oligomers of growing size and, in the near-surface region of the zeolite crystal, of more or less extended oxide conglomerations, probably accompanied by massive structural damage and inclusion of alumosilicate matter.

4.2. Relation between structure and catalytic performance of Fe sites

Catalysts of the ILIE series provide, to our knowledge, the best SCR activities published for Fe-ZSM-5 in the literature so far (excluding [9], which has not been reproduced). With isobutane, Fe-Z(0.3) gives a peak NO conversion of $> 86\%$ at 623 K (Fig. 1), whereas other authors report 78–86% for Fe-ZSM-5 made via the CVD route (including those additionally promoted by La) [11,47] with Fe contents of ca. 5%. It is true that application of a moist feed increases the peak conversion over La-Fe-ZSM-5 to 90% [47]. However, at higher temperatures, this catalyst suffers the same loss in NO conversion as other Fe-ZSM-5 materials prepared via the CVD route, ending up at 40–50% conversion at 723–773 K (see, e.g., [11]) where Fe-Z(0.3) still converts $> 70\%$ of the NO. This excellent behavior at higher temperatures is a key feature of the latter. In NH_3-SCR, Fe-Z(1.2) compares well with a Fe-ZSM-5 of 1.9 wt% made by Long and Yang [30] by the same preparation route as the one we have adopted here. In a run at 1,100,000 h^{-1}, Fe-Z(1.2) achieved or exceeded the conversions reported in [30] at all temperatures with a slightly lower Fe content. As in case of isobutane-SCR, it has been shown very recently that Fe-ZSM-5 can be effectively promoted by rare-earth ions, in this case ceria [48].

The availability of quantitative estimates for the amounts of Fe species in the catalysts employed prompted us to correlate SCR rates with these data. Since the rates have been measured far outside the differential range of conversions, assumptions regarding the rate law had to be made to allow the correlation of rate constants with the quantity of sites. A first-order rate law was assumed for both reactions. For NH_3-SCR, this is fully in agreement with kinetic measurements of Huang et al. [49], who found orders of ~ 1 for NO and ~ 0 for NH_3. For hydrocarbon-SCR, there

are hardly any kinetic measurements available, except for the methane reductant. There, the sum of reaction orders of NO and methane (for equimolar feed) is often found to be around 1, but in some reports it is considerably higher (cf. [50]).

Fig. 12a shows the results for different correlation attempts for isobutane-SCR at 523 K, which is well below the conversion maximum. It is clear from this figure that the rate constant correlates best with the sum of the iron in isolated and oligomeric sites, whereas there is no proportionality with the concentration of the oligomeric clusters alone (Fig. 12, a2). Therefore, a major contribution of the isolated sites can be identified. The correlation of the rate constant with the concentration of isolated sites yields a bent curve (Fig. 12, a1), which implies the participation of a second type of site, the oligomers. Given the fact that only one of the samples contains significant amounts of large aggregates, one might expect that the correlation with the total Fe does not differ much from that with the sum of oligomers and isolated sites. This is indeed the case; in fact, the correlation does not go through the origin, although the intercept is small (Fig. 12, a1). Apparently, the surfaces of the clusters do not contribute to the SCR reaction, which agrees with observations made by many other groups before.

For NH_3-SCR, similar conclusions can be drawn from the correlations in Fig. 12b. The attempt to correlate with Fe in oligomers alone fails (Fig. 12, b2). However, the best result is achieved here with the total Fe content (Fig. 12, b1), which is even better than that achieved with the sum of isolated and oligomeric sites (Fig. 12, b2). From this, it can be concluded that all accessible iron, probably including the surfaces of the oxide aggregates, participates in NH_3-SCR.

Despite the rather clear-cut results, these correlations should be taken with some caution. As mentioned above, the actual species concentrations may be influenced by a moderate systematic deviation, and the results of Fe-Z(1.2) may be additionally affected by the uncertainty about contributions of the clusters at lower wavelengths. Moreover, all "species" employed in the analysis represent in fact several sites, which may have different reactivities. Thus, there are three types of isolated sites, the different reduction behavior of which is demonstrated in Part II of this paper [32]. Hence, differences in their intrinsic SCR activities seem to be quite likely. The intrinsic activity of oligomers may be influenced by their nuclearities, and that of the aggregates by the state of their structural order. However, most of the conclusions suggested above may be also derived without reliance on the quantitative correlations shown in Fig. 12.

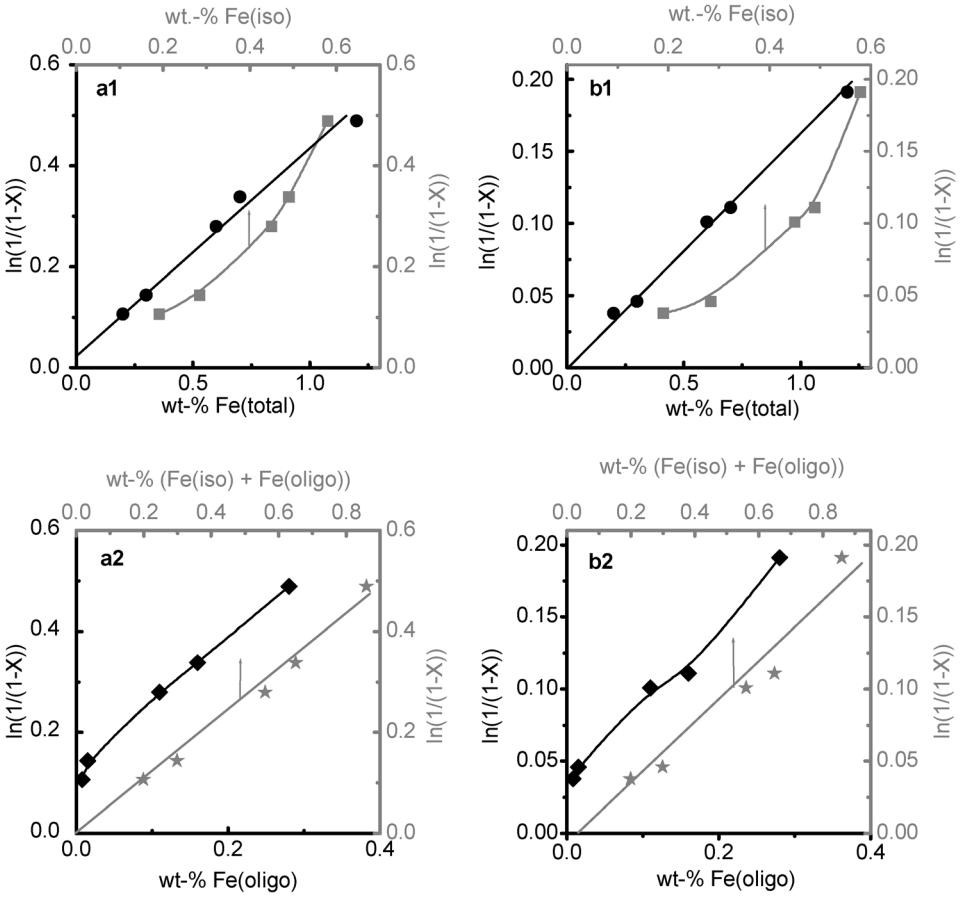

Fig. 12. Correlation of SCR rates (first-order rate constants) with the concentration of different Fe species detected by UV–vis spectroscopy. (a) SCR with isobutane at 523 K; (b) SCR of NO with ammonia at 523 K.

Thus, the conclusion about the activity of isolated sites in isobutane-SCR may be based also on the fact that the best catalyst (Fe-Z(0.3)) contains almost all of its iron in mononuclear entities, and that the dramatic increase in the concentration of oligomeric sites in Fe-Z(0.6) (Table 5) on the whole cause the catalytic behavior to deteriorate. However, a contribution of the oligomeric sites to the SCR cannot be conclusively identified from the present data on a qualitative basis because it is not possible to separate the assumed contributions of mononuclear and oligomeric sites qualitatively. If, however, the concentration of isolated sites in Fe-Z(1.2) is indeed overestimated (vide supra), a significant contribution of oligomers would have to be invoked to explain the further growing low-temperature conversion despite the decreasing concentration of isolated sites. With NH_3-SCR, the confirmation of the catalytic relevance of isolated sites follows the same lines drawn for isobutane-SCR; the dramatic increase in the concentration of oligomeric sites between Fe-Z(0.3) and Fe-Z(0.6) does not cause a corresponding jump in NO conversion (Fig. 3). It improves, however, the activity much more than the gradual growth of the isolated site concentration would justify, and the increase goes on up to Fe-Z(1.2). Therefore, the contribution of the oligomers to the SCR of NO is more obvious for the ammonia than for the isobutane reductant. Indeed, looking at NO conversions at higher temperatures suggests that they might possess a higher intrinsic activity in this reaction: when proceeding from Fe-Z(0.3) to Fe-Z(0.6), which increases the mononuclear sites moderately and adds oligomer sites in an amount still much below that of the isolated sites, the NO conversion jumps from 18 to 53% at 673 K, and from 30 to 78% at 723 K (Fig. 3). A contribution of the particles cannot be identified from qualitative considerations, but given a particular activity of the oligomers, a contribution of the particle surfaces should not be ruled out, although it would be marginalized by the contributions of the higher disperse entities.

As for the catalytic contribution of clustered structures, our results permit us to draw an additional conclusion that leads to a unified understanding of the catalytic behavior of Fe-ZSM-5 in both reactions. The increase in the concentration of clustered sites from Fe-Z(0.3) to Fe-Z(1.2) leads to a continuous deterioration of the catalytic behavior in isobutane-SCR, except for the lowest temperature studied (Fig. 1). This is obviously due to an increased tendency toward the unselective total oxidation of isobutane. The bridging oxygen, be it in binuclear complexes as favored by [10,11,16,17] or in oligomers of a wide range of nuclearities as suggested in [13], probably participates in the SCR at low temperatures, but it is obviously not selective for NO, but attacks the reductant unselectively at higher temperature.

In NH_3-SCR, the same trend can be seen, but at much higher temperatures. With the catalysts containing almost exclusively isolated sites, unselective NH_3 oxidation cannot be detected up to 873 K. With increasing content of clustered sites, the NH_3 conversion starts to exceed the NO conversion under more and more moderate conditions. Our in situ spectroscopic studies show indeed that under reaction conditions, the iron sites are much more reduced in isobutane-SCR feed than in NH_3-SCR feed; that is, the interaction of NH_3 with the iron is much weaker [32]. This explains why clustered sites exhibit a constructive role in NH_3-SCR but not in isobutane-SCR, and it forms the basis of quite different optimization strategies for Fe-ZSM-5 in these reactions. For isobutane-SCR, the concentration of isolated sites has to be increased, avoiding clustered sites. For NH_3-SCR, a high dispersion of iron should be sought as well, but the Fe content may be increased without limitations imposed by cluster formation, because small clusters are favorable in this reaction.

5. Conclusions

Fe-ZSM-5 catalysts with low Fe content (0.2–1.2 wt%) were prepared by exchange of Na-ZSM-5 with Fe^{2+} ions that were formed by the dissolution of iron metal in acidic medium. The structure of the Fe species was characterized by various physicochemical techniques (UV–vis, EPR, X-ray absorption spectroscopy, TPR, TEM) and related to their activity in the selective catalytic reduction of NO by isobutane or by ammonia. It was found that at Fe contents less than or equal to 0.3 wt%, ca. 95% of the iron was present as mononuclear sites of different coordination, whereas mononuclear sites coexisted with oligomeric entities at 0.6–0.7 wt% Fe, and additionally with large, poorly ordered Fe oxide aggregates at 1.2% Fe.

The catalysts prepared proved highly active in both SCR reactions, competing favorably with catalysts prepared by chemical vapor deposition of $FeCl_3$ into H-ZSM-5, which contain much more iron. By correlation of the activities with the concentration of different Fe sites observed, it was established that mononuclear Fe ions are active sites for both SCR reactions. At the same time, oligomers contribute to both reactions as well, probably with a higher intrinsic activity than the mononuclear sites in NH_3-SCR. On the other hand, oligomers (and aggregate surfaces) are more active in the unselective oxidation of the reductant, which limits the temperature window of selective NO reduction. This unselective attack by clustered species occurs at low temperatures in the case of the isobutane reductant; hence, the catalyst performing best in this reaction was almost void of clusters. With the NH_3 reductant, the unselective attack occurred at much higher temperature, and the limitation of the selective temperature region was of little practical importance. Hence, the best catalyst for NH_3-SCR was the one with the highest Fe content.

Acknowledgment

We thank the Deutsche Forschungsgemeinschaft for financial support (grants Br 1380/7-1 and Gr 1447/7-1).

References

[1] G.I. Panov, G.A. Sheveleva, A.S. Kharitonov, V.N. Romannikov, L.A. Vostrikova, Appl. Catal. A 82 (1992) 31.
[2] G.I. Panov, M.A. Uriarte, M.A. Rodkin, V.I. Sobolev, Catal. Today 41 (1998) 365.
[3] M. Kögel, V.H. Sandoval, W. Schwieger, A. Tissler, T. Turek, Catal. Lett. 51 (1998) 23.
[4] J. Pérez-Ramirez, F. Kapteijn, G. Mul, X. Xu, J.A. Moulijn, Catal. Today 76 (2002) 55.
[5] S. Kameoka, K. Yuzaki, T. Takeda, S. Tanaka, S. Ito, T. Miyadera, K. Kunimori, PCCP 2 (2001) 256.
[6] A. Ma, W. Grünert, Chem. Commun. (1999) 71.
[7] Q. Sun, Z.X. Gao, H.-Y. Chen, W.M.H. Sachtler, J. Catal. 201 (2002) 89.
[8] R.Q. Long, R.T. Yang, J. Am. Chem. Soc. 121 (1999) 5595.
[9] X. Feng, W.K. Hall, Catal. Lett. 41 (1996) 45.
[10] H.-Y. Chen, W.M.H. Sachtler, Catal. Today 42 (1998) 73.
[11] A.A. Battiston, J.H. Bitter, D.C. Koningsberger, J. Catal. 218 (2003) 163.
[12] R.W. Joyner, M. Stockenhuber, Catal. Lett. 45 (1998) 15.
[13] F. Heinrich, C. Schmidt, E. Löffler, M. Menzel, W. Grünert, J. Catal. 212 (2002) 157.
[14] Q. Zhu, R.M. van Teeffelen, R.A. van Santen, E.J.M. Hensen, J. Catal. 221 (2004) 575.
[15] R.Q. Long, R.T. Yang, J. Catal. 201 (2001) 145.
[16] P. Marturano, L. Drozdova, A. Kogelbauer, R. Prins, J. Catal. 192 (2000) 236.
[17] A.A. Battiston, J.H. Bitter, F.M.F. de Groot, A.R. Overweg, O. Stephan, J.A. van Bokhoven, P.J. Kooyman, V. van der Sperk, G. Vanko, D.C. Koningsberger, J. Catal. 213 (2003) 251.
[18] L. Kiwi-Minsker, D.A. Bulushev, A. Renken, J. Catal. 219 (2003) 273.
[19] J.F. Jia, K.S. Pillai, W.M.H. Sachtler, J. Catal. 221 (2004) 119.
[20] E.J.M. Hensen, Q. Zhu, R.A. van Santen, J. Catal. 220 (2003) 260.
[21] B. Wichterlova, Z. Zobalik, J. Dedecek, Appl. Catal. B 41 (2003) 97.
[22] Q. Zhu, B.L. Mojet, E.J.M. Hensen, P.C.M.M. Magusin, R.A. van Santen, Catal. Lett. 81 (2002) 205.
[23] Z. Sobalik, A. Vondrova, Z. Tvaruskova, B. Wichterlova, Catal. Today 75 (2002) 347.
[24] M. Santhosh Kumar, M. Schwidder, W. Grünert, A. Brückner, J. Catal. 227 (2004) 384.
[25] E.J.M. Hensen, Q. Zhu, M.M.R.M. Hendrix, A.R. Overweg, P.J. Kooyman, M.V. Sychev, R.A. van Santen, J. Catal. 221 (2004) 560.
[26] F. Heinrich, C. Schmidt, E. Löffler, W. Grünert, Catal. Comm. 2 (2001) 317.
[27] J. Pérez-Ramirez, M. Santhosh Kumar, A. Brückner, J. Catal. 223 (2004) 13.
[28] J. Pérez-Ramirez, F. Kapteijn, A. Brückner, J. Catal. 218 (2003) 234.
[29] M. Schwidder, F. Heinrich, M.S. Kumar, A. Brückner, W. Grünert, Stud. Surf. Sci. Catal. 154 (2004) 2484.
[30] R.Q. Long, R.T. Yang, Catal. Lett. 74 (2001) 201.
[31] M. Schwidder, PhD Thesis, Bochum, 2004.
[32] M. Santhosh Kumar, M. Schwidder, W. Grünert, A. Brückner, in preparation.
[33] M. Schwidder, M. Santhosh Kumar, A. Brückner, W. Grünert, Chem. Commun. (2005) 805.
[34] E.P. Barrett, L.G. Joyner, P.P. Halenda, J. Am. Chem. Soc. 73 (1951) 373.
[35] K.V. Klementiev, VIPER for Windows (Visual Processing in EXAFS Researches), freeware, http://www.desy.de/~klmn/viper.html.
[36] A.L. Ankudinov, B. Ravel, J.J. Rehr, S.D. Conradson, Phys. Rev. B 58 (1998) 7565.
[37] M. Wark, A. Brückner, T. Liese, W. Grünert, J. Catal. 175 (1998) 48.
[38] G. Piehl, T. Liese, W. Grünert, Catal. Today 54 (1999) 401.
[39] F. Heinrich, PhD Thesis, Bochum, 2002.
[40] J. Vedrine, et al., Catal. Today 56 (2000) 329.
[41] O.J. Wimmers, P. Arnoldy, P.A. Moulijn, J. Phys. Chem. 90 (1986) 1331.
[42] S. Bordiga, R. Buzzoni, F. Geobaldo, C. Lamberti, E. Giamello, A. Zecchina, G. Leofanti, G. Petrini, G. Tozzola, G. Vlaic, J. Catal. 158 (1996) 486.
[43] D. Kaucky, J. Dedecek, B. Wichterlova, Micropor. Mesopor. Mater. 31 (1999) 75.
[44] R. Zysler, D. Fiorani, J.L. Dormann, A.M. Testa, J. Magn. Magn. Mater. 133 (1994) 71.
[45] R. Berger, J.-C. Bissey, J. Liava, H. Daubric, C. Estournès, J. Magn. Magn. Mater. 234 (2001) 535.
[46] J. Liava, R. Berger, J. Magn. Magn. Mater. 205 (1999) 328.
[47] H.-Y. Chen, W.M.H. Sachtler, Catal. Lett. 50 (1998) 125.
[48] G. Carja, G. Delahay, C. Signorile, B. Coq, Chem. Commun. (2004) 1404.
[49] H.Y. Huang, R.Q. Long, R.T. Yang, Appl. Catal. A 235 (2002) 241.
[50] T. Sowade, F.-W. Schütze, H. Berndt, W. Grünert, Chem. Eng. Technol. 27 (2004) 1277.